

Improved sampling patterns for accelerated diffusion spectrum imaging using compressed sensing

M. I. Menzel¹, J. I. Sperl¹, E. T. Tan², K. Khare², K. F. King³, X. Tao², C. J. Hardy², and L. Marinelli²

¹GE Global Research, Garching bei München, Germany, ²GE Global Research, Niskayuna, NY, United States, ³GE Healthcare, Waukesha, WI, United States

Introduction

Over the last decade, the study of diffusion properties by MRI methods has gained significant importance for understanding the central nervous system [1]. Among the most comprehensive methods, but also most time consuming, is the Nyquist sampling of q-space [2], known as diffusion spectrum imaging (DSI) [3]. Despite its large information content, fully-sampled DSI has not so far been commonly adopted in clinical practice due to scan time constraints. This motivated the acceleration of DSI using compressed sensing [4-7]. The output of a DSI experiment is the diffusion propagator for each sampled voxel, resulting in a six dimensional data space. The angular information encoded in the diffusion propagator is often made explicit through the computation of the orientation distribution function (ODF) [8]. Analogously, the radial information in q-space has been the subject of numerous studies in the literature [1]. The radial component contains information about the nature of diffusion (i.e. free Gaussian, non-Gaussian, restricted), and it can be parameterized in a first approximation by the kurtosis expansion of the well known Stejskal-Tanner equation [9]. Acceleration of DSI can be achieved by undersampling q-space with random patterns. Compressed sensing can then be employed to reconstruct missing data points in q-space. The effect of choice of realization of the sampling pattern and of the CS reconstruction on derived quantities such as ODF and kurtosis were evaluated and compared to fully sampled data.

Methods

Simulations of 2D diffusion propagator data were performed using Matlab (Mathworks, Natick, MA, USA). The displacement signal for a two-fiber crossing was simulated with a sum of two separate Gaussian propagators, assuming no diffusional exchange between the different fibers, a fractional anisotropy (FA) of 0.85 and a 70° angle between the fibers. After comparison to random undersampling (data not shown) and to Poisson disk undersampling (data not shown), random Gaussian undersampling was chosen with its central points fully-sampled [4]. Covering q-space in 3D, echo-planar imaging DSI experiments on healthy volunteers were performed using a 3T GE MR750 MR scanner (GE Healthcare, Milwaukee, WI, USA), equipped with an 8 channel head coil ($TE = 141\text{ ms}$, $TR = 3\text{ s}$, 128×128 , $FOV = 25\text{ cm}$, $slice = 4\text{ mm}$, $b_{\max} = 10,000\text{ s/mm}^2$). To evaluate the dependence of CS reconstruction on the realization of the undersampled Gaussian pattern, 1000 different realizations drawn from a single distribution (identical parameters) were tested both with 2D (simulations) and 3D (volunteer brain data). The following properties of undersampled patterns were examined: effect of acceleration factor R ranging between $R=2.3 - 6$ in 2D and in 3D (data not shown); effect of size of centrally fully sampled region in 2D (Fig. 3); effect of sampling grid size both for constant diffusional displacement FOV and constant q_{\max} in 2D (data not shown). The quality of q-space reconstruction compared to the fully sampled ground truth was evaluated in 2D and 3D by direct point-wise correlation of q-space (data not shown), structural similarity index (SSIM) [10] of q-space in 3D (Fig. 2), and direct point-wise correlation of ODF after CS reconstruction in 2D (Fig. 3).

Results and Discussion

Fig. 1 a) depicts a specific 3D q-space sampling pattern; b) shows the fully sampled ground truth q-space (2D surface of central plane of 3D q-space); c) shows the corresponding undersampled q-space; d) depicts the reconstructed q-space after CS recon. While samples near the center of q-space remain relatively unchanged, there is a smoothing/denoising effect of CS recon for larger q . This effect is particularly pronounced for large R and in voxels within highly anisotropic regions of the brain: Fig. 2 depicts the SSIM of 3D q-space after CS reconstruction between undersampled q-space and ground truth using two different representative realizations of the random distribution on a $11 \times 11 \times 11$ grid, one instance (#134 out of 1000) is depicted in Fig. 1a). Depending on the shape of q-space for different regions in the brain, the SSIM between ground truth q-space and CS reconstructed q-space varies between the realizations of the pattern (left pattern: higher SSIM, right pattern: lower SSIM). The effect of CS reconstruction on derived quantities however might be more pronounced and may not be captured adequately by direct comparison of q-space. To this end, also the quality of ODF reconstruction based on realization of pattern was evaluated in 2D simulations and compared to ground truth. Fig. 3 depicts the comparison of 2D simulated fiber crossing (33×33 , $R=4$), with identical acceleration but larger fully sampled center.

Conclusion and Outlook

For small sampling matrix sizes in compressed sensing DSI, there is a dependence of CS reconstruction quality on the particular choice of sampling pattern. This may be expected as for small N the probability of a pattern that leads to coherent aliasing in CS reconstruction is not vanishingly small. The effect of these artifacts can be visually seen in the corresponding derived quantities. An evaluation of pattern quality via pair-wise correlation or SSIM is straightforward and fast, however a more accurate assessment may be obtained looking at transfer point spread functions. However, in vivo data is always contaminated by noise, so the ground truth is erroneous itself and any correlation of CS reconstructed data with it will be biased by this noise as well.

References

- [1] J. H. Jensen, et al., *NMR Biomed.*, vol. 23, pp. 659-660. [2] P. T. Callaghan, et al., *J. Magn. Reson. (1969)*, vol. 90, pp. 177-182, 1990. [3] V. J. Wedeen, et al., *MRM*, vol. 54, pp. 1377-1386, 2005. [4] M. I. Menzel, et al., *Proc. ISMRM*, p. 1698, 2010. [5] N. Lee, et al., *Proc ISMRM*, p. 1697, 2010. [6] K. Khare, et al., *ISMRM*, 2010. [7] K. Khare, et al., *IEEE Trans. Medical Imaging*, in review, 2010. [8] D. S. Tuch, *MRM*, vol. 52, pp. 1358-1372, 2004. [9] J. H. Jensen, et al., *MRM*, vol. 53, pp. 1432-1440, 2005. [10] W. Zhou, et al., *Image Processing, IEEE Transactions on*, vol. 13, pp. 600-612, 2004.

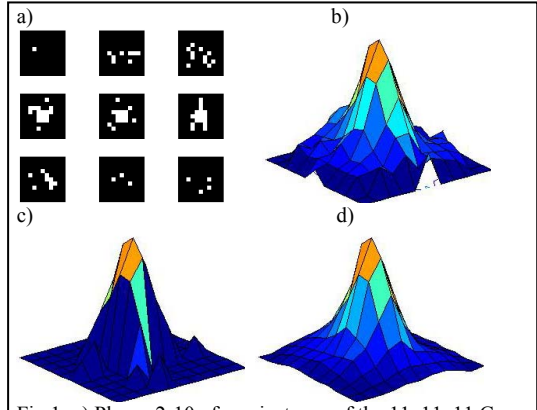


Fig 1: a) Planes 2-10 of one instance of the $11 \times 11 \times 11$ Gaussian undersampling pattern; b) fully sampled ground truth q-space (2D surface of central plane of 3D q-space); c) undersampled q-space; d) q-space after CS reconstruction.

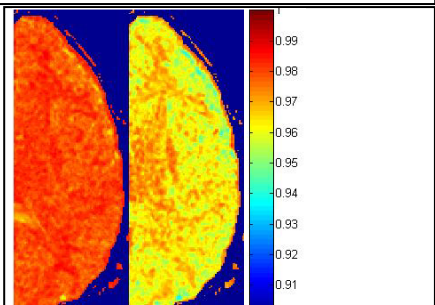


Fig 2: Evaluation of SSIM of 3D q-space data (fully sampled ground truth vs. under-sampled ($R=4$) and CS reconstructed) with different instances of the undersampling pattern: left: instance #889/1000; right: instance #134/1000.

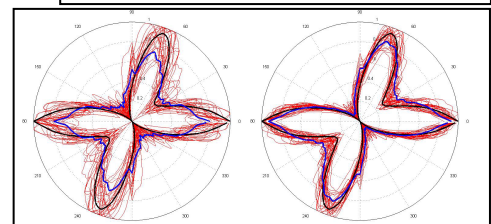


Fig 3: ODF of simulated 2D fiber crossing undersampled with Gaussian pattern reconstructed using CS (33×33 , $R=4$). 1000 instances of each undersampling scheme were tested. Black: ground truth ODF (fully sampled), blue: mean ODF after reconstruction from 1000 different patterns, red: ODF for individual instances with correlation coefficients to fully sampled larger than specified threshold: left: inner square 5×5 (correlation coefficient > 0.9); right: inner square 9×9 (correlation coefficients > 0.97).